JOURNAL OF MATERIALS SCIENCE 26 (1991) 5053–5059

Determination of the Al/Si distribution in synthetic $K_xMg_2Al_{4+x}Si_{5-x}O_{18}$ ($0 < x \leqslant 1$) cordierites by ^{29}Si and ^{27}Al MAS-NMR spectroscopy

J. SENEGAS
Laboratoire de Chimie du Solide du C.N.R.S., Université de Bordeaux I, 351 Cours de la Libération, 33405 Talence Cedex, France

A. R. GRIMMER, D. MULLER
Central Institute of Inorganic Chemistry, Academy of Sciences of the GDR, Adlershof, O-1199 Berlin, FRG

P. THOMAS D. MERCURIO, B. FRIT
Laboratoire de Chimie Minérale Structurale (U.A.-C.N.R.S. no. 320), Faculté des Sciences, 123 Avenue A. Thomas, 87060 Limoges Cedex, France

^{29}Si magic angle spinning-nuclear magnetic resonance study of three samples of potassium-substituted hexagonal cordierites with $K_xMg_2Al_{4+x}Si_{5-x}O_{18}$ formula ($x = 0.25, 0.50, 1$) has allowed the determination, in each case, of the distribution of aluminium and silicon atoms among the tetrahedral framework sites. It has been shown that the excess of aluminium compensating for the insertion of potassium within the hexagonal channels is accommodated by only the T(2) sites of the six-membered rings. A short-range order, which decreases with increasing potassium content, has been evidenced, in agreement with the results from the Rietveld refinement of neutron diffraction data.

1. Introduction

New alkali-substituted cordierites with formula $M_xMg_2Al_{4+x}Si_{5-x}O_{18}$ ($M = K, Cs; 0 < x \leqslant 1$) have been synthesized both by glass crystallization and by the sol–gel method [1–3]. They all crystallize with the hexagonal symmetry (high-temperature disordered polymorph; space group: P6/mcc) and exhibit remarkable thermal properties [4–9]. For instance, the $K_{0.5}Mg_2Al_{4.5}Si_{4.5}O_{18}$ compound has the lowest mean thermal expansion coefficient ever observed in such materials ($\alpha \approx 0.4 \times 10^{-6}\ K^{-1}$ between 293 and 1100 K) [3, 6].

The structural characteristics at room temperature of three compounds of the $K_xMg_2Al_{4+x}Si_{5-x}O_{18}$ series ($x = 0.25, 0.50, 1.0$) have been deduced from Rietveld refinements of neutron diffraction data [5, 10]. In each case the polyhedra arrangement (Fig. 1) is typical of the hexagonal pure cordierite framework. It consists of 6-membered rings of $T(2)O_4$ tetrahedra, centred at the origin, lying in the xOy plane, stacked one above the other and successively rotated 30° relative to each other. Rings are linked together, laterally and vertically, by $T(1)O_4$ tetrahedra and MgO_6 octahedra which, by sharing edges, form a two-dimensional network of large overlapping 12-membered rings [$T(1)O_4$–MgO_6] parallel to xOy.

Ideal [$T(1)O_4$–MgO_6] rings would not be large enough to fit around the 6-membered $T(2)O_4$ rings. They are therefore severely distorted: the $T(1)O_4$ tetrahedra are elongated along one of their $\bar{4}$ axes ($//xOy$) and the MgO_6 octahedra are stretched isotropically along the same plane.

The ring stacking produces large hexagonal channels, parallel to Oz, in which potassium atoms are statistically distributed among the 4c ($0\,0\,z$) positions.

The experimental values reported in Table I indicate (i) an increase of the average values $\langle T\text{–}O \rangle$ mainly due to the clear increase of the T(2)–O(2) distances, which is quite logical because the O(2) atoms are the only oxygen atoms directly linked to potassium atoms; (ii) a disparity in the T(2)–O(2) distances within each tetrahedron of the 6-membered rings, a disparity previously observed by Meagher and Gibbs [11] for a pure hexagonal cordierite (indialite) and which disappears with increasing aluminium contents. Such a phenomenon surely results from the existence of an Al/Si short-range order whose nature changes with aluminium content.

X-ray and even neutron diffraction techniques are generally of little value in determining the character and occupancy of structural sites in materials that lack long-range order, especially in the case of cordierites,

0022–2461/91 $03.00 + .12

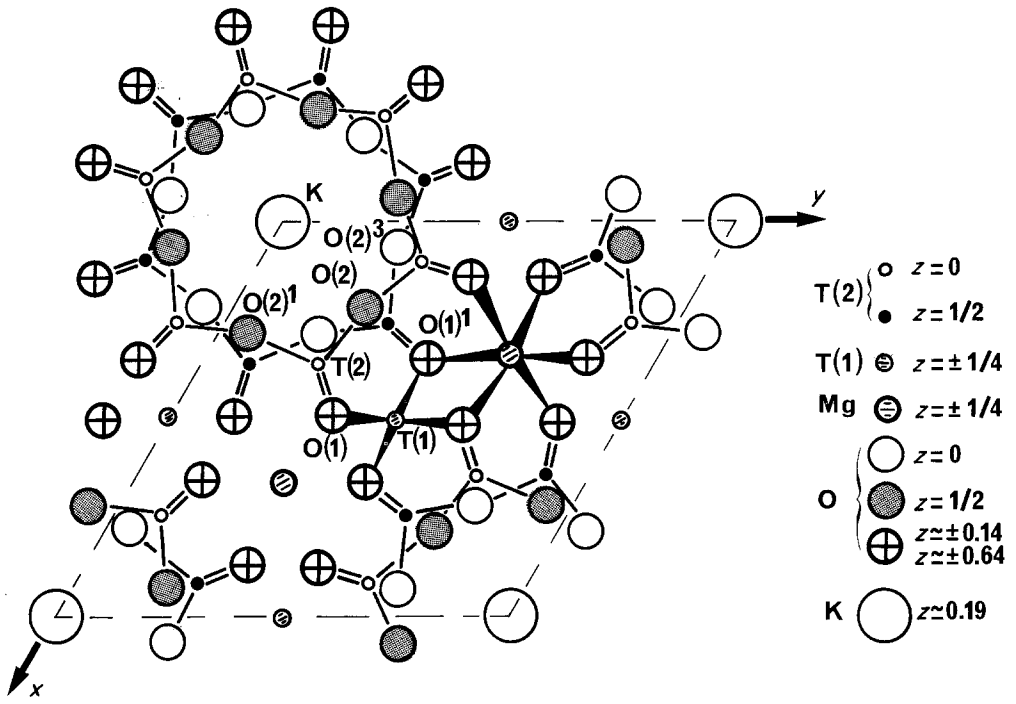

Figure 1 Projection along the *c*-axis of the $K_{0.5}Mg_2Al_{4.5}Si_{4.5}O_{18}$ cordierite.

TABLE I Main cation–anion distances and occupancies for tetrahedral sites T(1) and T(2) in some $K_xMg_2Al_{4+x}Si_{5-x}O_{18}$ hexagonal cordierites (powder neutron diffraction study) [10]. Notation of atoms are those given in Fig. 1

Occupancies (%) and distances (nm)	$x = 0.25$	$x = 0.5$	$x = 1$
$\tau_{Si}^{T(1)}$	50	50	41
$\tau_{Si}^{T(2)}$	54(3)	50(2)	46(2)
K–O(2) × 6	0.3140(9)	0.3160(7)	0.3146(3)
K–O(2)^3 × 6	0.4054(9)	0.4037(7)	0.4007(3)
⟨K–O(2)⟩	0.3597	0.3598	0.3576
K–O(1) × 6	0.4250(9)	0.4261(6)	0.4271(3)
K–O(1)^1 × 6	0.4567(9)	0.4565(6)	0.4567(3)
⟨K–O(1)⟩	0.4408	0.4413	0.4419
T(1)–O(1) × 4	0.1725(2)	0.1722(2)	0.1729(1)
T(2)–O(1) × 2	0.1683(3)	0.1669(3)	0.1678(2)
T(2)–O(2)	0.1606(4)	0.1621(3)	0.1639(2)
T(2)–O(2)^1	0.1633(4)	0.1656(3)	0.1644(2)
⟨T(2)–O(2)⟩	0.1619	0.1638	0.1641
⟨T(2)–O⟩	0.1651	0.1654	0.1660

because aluminium and silicon atoms have similar (X-ray) or nearly similar (neutron) scattering factors. In fact, the occupancies of T(1) and T(2) sites do not change significantly (see Table I). High-resolution solid state ^{29}Si magic angle spinning–nuclear magnetic resonance (MAS–NMR), on the other hand, is capable of detecting the relative amounts of the five possible Si(*n*Al) structural groups ($n = 0$–4 is the number of tetrahedral aluminium atoms joined, by oxygen bridges, to the central silicon atoms) [12–15]. In order to establish the precise nature of the Al/Si distribution among the tetrahedral framework sites, we have undertaken a MAS–NMR study of the same potassium-substituted samples.

TABLE II Experimental parameters for the recording of the ^{29}Si and ^{27}Al NMR spectra. (ν_0 = resonance frequency, D_1 = pulse width, D_0 = delay time, N_s = number of scans, ν_s = spinning frequency)

	ν_0(MHz)	D_1 (μs)	D_0(s)	N_s	ν_s(kHz)
^{29}Si	79.5	12	5	1000	3.5
^{27}Al	104.2	2	0.3	1000	5.4

2. Experimental procedure

Glassy pieces with composition $K_xMg_2Al_{4+x}Si_{5-x}O_{18}$ ($x = 0.25$, 0.50, 1.0) were obtained by melting and water-quenching weighed quantities of reagent-grade SiO_2xH_2O, Al_2O_3, MgO and K_2CO_3. After ball-milling for 2 h, the powders were heated in air (1273 K/2 h + 1333 K/2 h) in order to ensure complete crystallization. X-ray fluorescence analysis did not show any significant deviation from the nominal compositions.

High-resolution ^{29}Si and ^{27}Al NMR spectra were recorded at 293 K on a Bruker MSL 400 spectrometer by using the MAS technique (54.7°) and the CYCLOPS program. The main recording parameters are given in Table II. All ^{29}Si chemical shifts are given from Q_8M_8 (abbreviation for $[(CH_3)_3Si]_8Si_8O_{20}$), and ^{27}Al chemical shifts from acidified (HCl) aqueous solution of $AlCl_3$. Deconvolutions of the experimental spectra were calculated by using Gaussian line shapes and a special program, LINESIM [16].

3. Results

3.1. ^{29}Si spectra

Fig. 2 shows ^{29}Si MAS–NMR spectra obtained for the three compositions studied. Each spectrum displays

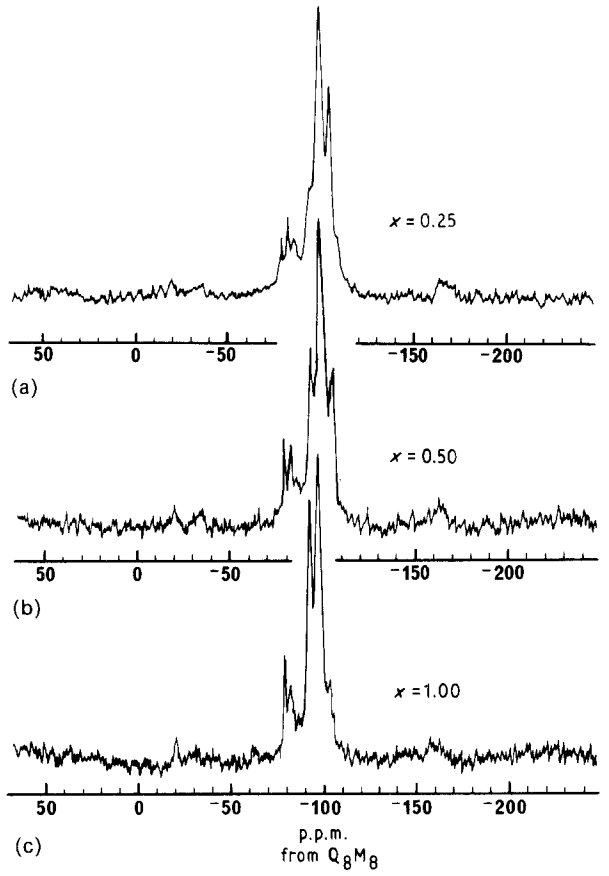

Figure 2 ^{29}Si MAS–NMR spectra of $K_xMg_2Al_{4+x}Si_{5-x}O_{18}$ cordierites: (a) $x = 0.25$, (b) $x = 0.50$, (c) $x = 1.0$.

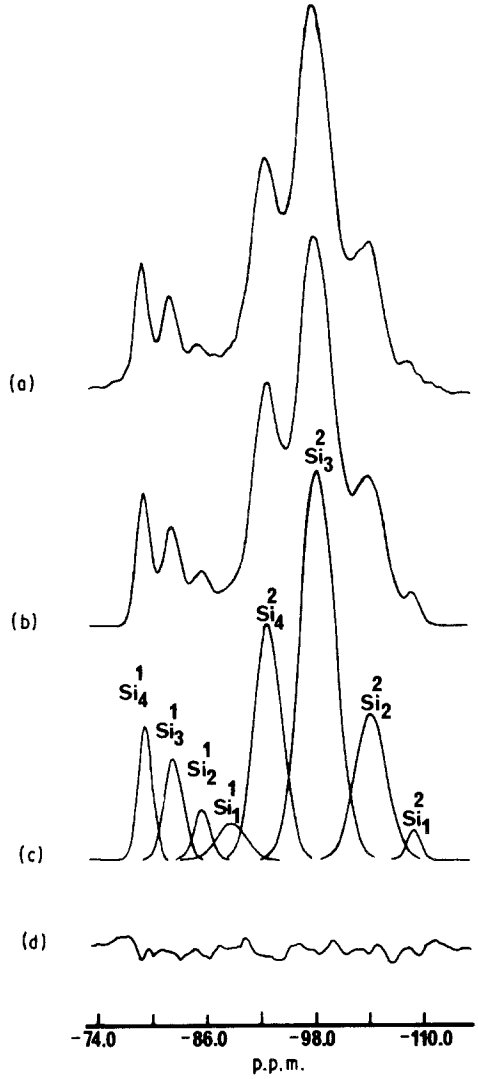

Figure 3 Deconvolution of the ^{29}Si MAS–NMR signal $K_{0.5}Mg_2Al_{4.5}Si_{4.5}O_{18}$ using Gaussian line shapes for the sample. (a) Experimental spectrum, (b) simulated spectrum, (c) Gaussian peaks used, (d) residue.

two distinct sets of well-resolved peaks, in the chemical shift ranges -79 to -90 and -93 to -109 p.p.m., which can be assigned, as proposed by Fyfe *et al.* [13] for pure cordierite, to silicon atoms in the T(1) and T(2) tetrahedral sites, respectively. These different peaks are denoted Si_n^1 with $0 \leqslant n \leqslant 4$ for the silicon atoms, in the T(1) site and linked to n aluminium atoms through bridging oxygen atoms, and Si_n^2 with $0 \leqslant n \leqslant 4$ for the silicon atoms, in the T(2) site and linked to n aluminium atoms.

For each of the two types of sites (T(1) and T(2)), a maximum of five ^{29}Si peaks are theoretically possible, namely Si_0, Si_1, Si_2, Si_3 and Si_4. It should be noted that for each site the Si_0 peaks are not observed, which indicates that all silicon atoms are linked to at least one aluminium atom.

Deconvolutions of the spectra using Gaussian line shapes give the relative intensity of each peak. A close fit between the observed and simulated spectra is generally obtained (Fig. 3). A more or less evident shoulder is, however, systematically observed on the left part of each peak (see for instance the Si_2^2 peak on Fig. 3) indicating its splitting into a doublet. This splitting could result from the existence of two slightly different pseudo-ordered microdomains within these "order-modulated" structures [11, 13, 15].

The study of these ordered microdomains, the extent of which is strongly dependent on the thermal history of the samples [13], will be the subject of further investigations.

3.2. ^{27}Al spectra

The ^{27}Al spectra are shown in Fig. 4. Contrary to the ^{29}Si spectra, their profile does not change significantly with aluminium content, which is quite logical, because only one strong peak, shifted 50 p.p.m. from the $Al(H_2O)_6^{3+}$ reference, characterizes the tetrahedrally coordinated aluminium atoms.

In addition, some small and ill-defined peaks are observed. They are composed of (i) spinning sidebands, symmetrically distributed on each side of the central peak and due to incompletely averaged second-order quadrupole interactions, and (ii) a small line, shifted 15 p.p.m., indicated by an arrow on Fig. 4, and characteristic of aluminium atoms in octahedral coordination, i.e. corresponding to the small amounts of alumina and mullite revealed by the X-ray analysis.

3.3. Exploitation of the spectra

The relative intensities, $I_{Si_n^1}$ and $I_{Si_n^2}$, their sum being normalized to 100

$$\left(\sum_{n=1-4} (I_{Si_n^1} + I_{Si_n^2}) = 100 \right)$$

are reported in Table III.

TABLE III ^{29}Si chemical shifts, Δ, and peak intensities, I (% of the whole signal), for the various samples studied

		T(1) site: x =			T(2) site: x =		
		0.25	0.50	1.00	0.25	0.50	1.00
Si_1	Δ (p.p.m.)	− 87.5	− 89.2	− 89.5	− 108.8	− 107.5	− 107.7
	I(%)	3.8	2.7	3.8	3.1	2.2	1.4
Si_2	Δ (p.p.m.)	− 85.0	− 85.8	− 86.3	− 105.2	− 104.7	− 103.3
	I(%)	4.4	3.3	3.9	25.5	17.8	12.5
Si_3	Δ (p.p.m.)	− 82.6	− 82.6	− 82.9	− 100.1	− 98.8	− 98.1
	I(%)	5.6	5.3	6.2	40.6	44.6	35.6
Si_4	Δ (p.p.m.)	− 79.3	− 79.4	− 80.1	− 94.0	− 93.5	− 93.3
	I(%)	2.7	4.6	7.2	14.3	19.5	29.4
$\sum_{n=1-4} I_{Si_n}$		16.5	15.9	21.1	83.5	84.1	78.9

TABLE IV Repartition of the tetrahedral sites in the disordered high-temperature hexagonal form of cordierite (nine tetrahedral sites per $K_xMg_2Al_{4+x}Si_{5-x}O_{18}$ formula unit)

Sites	Linkages per tetrahedron
3 T(1) (6-membered rings)	4 T(2)
6 T(2) (12-membered rings)	2 T(1) + 2 T(2)

The percentage of the total silicon in each tetrahedral site is given by

$$[Si]^{T(1)} = \sum_{n=0-4} I_{Si_n^1} \quad \text{for the T(1) site} \quad (1)$$

$$[Si]^{T(2)} = \sum_{n=0-4} I_{Si_n^2} \quad \text{for the T(2) site} \quad (2)$$

Considering the distribution of tetrahedral sites within the hexagonal lattice indicated in Table IV, the numbers of aluminium and silicon atoms per unit formula $K_xMg_2Al_{4+x}Si_{5-x}O_{18}$ and for each site are calculated as follows (Table V)

$$N_{Si}^{T(1)} = (5 - x)\,[Si]^{T(1)} \quad (3)$$

$$N_{Si}^{T(2)} = (5 - x)\,[Si]^{T(2)} \quad (4)$$

$$N_{Al}^{T(1)} = 3 - N_{Si}^{T(1)} \quad (5)$$

$$N_{Al}^{T(2)} = 6 - N_{Si}^{T(2)} \quad (6)$$

The percentage of the total aluminium in each tetrahedral sites is then given by

$$[Al]^{T(1)} = N_{Al}^{T(1)}/4 + x \quad \text{for the T(1) site} \quad (7)$$

$$[Al]^{T(2)} = N_{Al}^{T(2)}/4 + x \quad \text{for the T(2) site} \quad (8)$$

The measured intensities of the various Si_n^1 and Si_n^2 peaks are compared in Table VI with those calculated for statistically random ordered non-Loewensteinian samples (i.e. in which the partition of aluminium and silicon atoms between the three T(1) and six T(2) sites is chosen to be identical with that found experimentally). Details of these calculations are given in the Appendix.

For aluminosilicate structures, it has been shown [13] that a Si/Al ratio may be derived from equation

$$\left[\frac{Si}{Al}\right]_{NMR} = \frac{\sum_{n=1-4} I_{Si_n}}{0.25 \sum_{n=1-4} n I_{Si_n}} \quad (9)$$

with

$$I_{Si_n} = I_{Si_n^1} + I_{Si_n^2} \quad (10)$$

If there are no Al–O–Al units present, this formula accurately reflects the actual Si/Al ratio of the lattice: $[Si/Al]_{actual} = (5 - x)/(4 + x)$. Following Fyfe *et al.* [13] the number of Al–O–Al linkages per $Al_{4+x}Si_{5-x}$ unit formula is then given by

$$N_{Al-O-Al} = 8 + 2x - \frac{10 - 2x}{[Si/Al]_{NMR}} \quad (11)$$

and the number of Al–O–Al linkages per aluminium atom by

$$N_{Al-O-Al}/N_{Al} = 2 - \frac{2[Si/Al]_{actual}}{[Si/Al]_{NMR}} \quad (12)$$

The corresponding values are reported in Table VII.

TABLE V Percentage and number of silicon and aluminium atoms in the two tetrahedral sites T(1) and T(2) for the three samples studied and for a pure hexagonal cordierite annealed 6 h at 1458 K[a]

x	Unit formula	T(1) sites					T(2) sites				
		[Si]	[Al]	N_{Si}	N_{Al}	N_{Si}/N_{Al}	[Si]	[Al]	N_{Si}	N_{Al}	N_{Si}/N_{Al}
0[a]	Al_4Si_5	15.6	55.5	0.780	2.220	0.351	84.4	44.5	4.220	1.780	2.37
0.25	$Al_{4.25}Si_{4.75}$	16.5	52.14	0.784	2.216	0.354	83.5	47.86	3.966	2.034	1.950
0.50	$Al_{4.50}Si_{4.50}$	15.9	50.77	0.715	2.286	0.313	84.1	49.24	3.784	2.216	1.708
1.0	Al_5Si_4	21.1	43.12	0.844	2.156	0.391	78.9	56.88	3.156	2.844	1.110

[a] From [13].

TABLE VI Measured (Exp.) and calculated (Th.) for a random Si/Al distribution (see Appendix) spectral intensities, normalized to a total of 100, of the various $Si_{n(Al)}$ signals, for the three samples studied and for a pure hexagonal cordierite annealed 6 h at 1458 K

x	Unit formula		T(1) sites Si_0	Si_1	Si_2	Si_3	Si_4	T(2) sites Si_0	Si_1	Si_2	Si_3	Si_4
0[a]	Al_4Si_5	Exp	0	1.1	2.2	4.3	8.0	0	2.0	20.3	51.3	10.8
		Th[b]	3.8	6.4	4.1	1.1	0.1	2.9	18.5	37.0	22.2	4.1
0.25	$Al_{4.25}Si_{4.75}$	Exp	0	3.8	4.4	5.6	2.7	0	3.1	25.5	40.6	14.3
		Th[b]	3.2	6.5	5.0	1.7	0.2	2.5	16.6	35.0	24.1	5.2
0.50	$Al_{4.50}Si_{4.50}$	Exp	0	2.7	3.3	5.3	4.6	0	2.2	17.8	44.6	19.5
		Th[b]	2.5	5.9	5.2	2.0	0.3	1.9	14.4	34.2	26.8	6.7
1.0	Al_5Si_4	Exp	0	3.8	3.9	6.2	7.2	0	1.4	12.5	35.6	29.4
		Th[b]	1.6	5.8	7.9	4.8	1.1	1.7	12.0	28.5	27.4	9.1

[a] From [13].
[b] Rounded to one decimal.

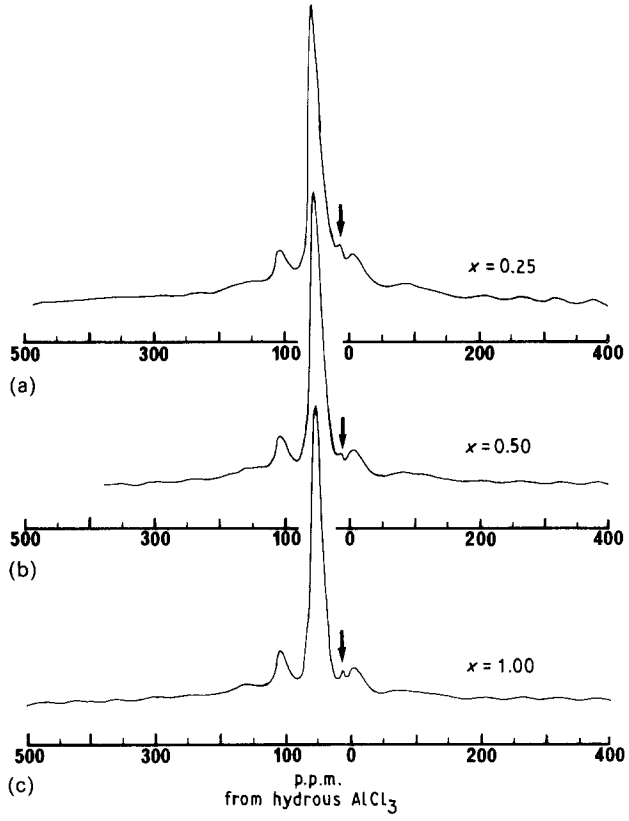

Figure 4 ^{27}Al MAS–NMR spectra of $K_xMg_2Al_{4+x}Si_{5-x}O_{18}$ cordierites: (a) $x = 0.25$, (b) $x = 0.50$, (c) $x = 1.00$.

4. Discussion

In all the samples and like in the pure cordierite samples previously studied [13] the aluminium and silicon atoms are not equally distributed among the two tetrahedral sites: the larger T(1) tetrahedra logically contain more aluminium than silicon atoms (about 2Al:1 Si), whereas the T(2) tetrahedra are mainly occupied by silicon atoms. The evolution of this partitioning with the increasing potassium content is shown in Fig. 5. It is in perfect accordance with the results obtained by Fyfe *et al.* [13] for a pure hexagonal cordierite annealed for 6 h at 1458 K (i.e. subjected to nearly the same thermal treatment as our samples), and clearly indicates that the aluminium excess compensating for the potassium insertion is accommodated by only the T(2) sites (the N_{Si}/N_{Al} ratio of the T(2)-site decreases from 2.37, in pure cordierite, to 1.11 when $x = 1$, whereas that of the T(1) site remains nearly constant). It justifies why the mean T(2)–O distance increases more than the mean T(1)–O distance when the potassium content increases (see Table I).

As in the case of pure cordierites, Al–O–Al linkages are observed in each sample (Table VII). Their number quite logically increases with the increasing aluminium content, but remains systematically smaller than

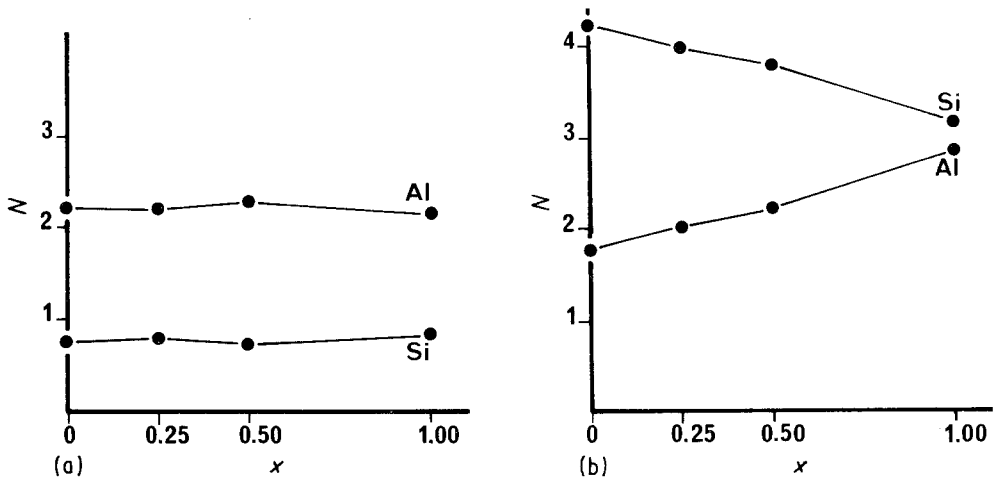

Figure 5 Evolution with potassium content, x, of the number of silicon and aluminium atoms in (a) T(1) and (b) T(2) tetrahedral sites. (The values for $x = 0$ are those given by Fyfe *et al.* [13]).

TABLE VII Measured (Exp) and calculated (Th) Si/Al ratios, numbers of Al–O–Al linkages and $N_{Si}^{T(2)}/N_{Si}^{T(1)}$ ratios, for the three samples studied and for a pure hexagonal cordierite annealed 6 h at 1458 K

x	Unit formula	$\left[\frac{Si}{Al}\right]_{actual}$	$\left[\frac{Si}{Al}\right]_{NMR}$	$N_{Al-O-Al}$	Exp./Th.	$N_{Al-O-Al}$ per Al	$\frac{N_{Si}^{T(2)}}{N_{Si}^{T(1)}}$	
0[a]	Al_4Si_5	1.250	1.38	0.74	0.23	0.18	5.41	Exp.
			2.06	3.16		0.79		Th.
0.25	$Al_{4.25}Si_{4.75}$	1.118	1.46	1.99	0.54	0.47	5.06	Exp.
			1.98	3.69		0.87		Th.
0.50	$Al_{4.5}Si_{4.5}$	1.0	1.36	2.41	0.52	0.53	5.29	Exp.
			1.87	4.18		0.93		Th.
1.0	Al_5Si_4	0.8	1.29	3.81	0.70	0.76	3.73	Exp.
			1.75	5.44		1.09		Th.

[a] From [13].

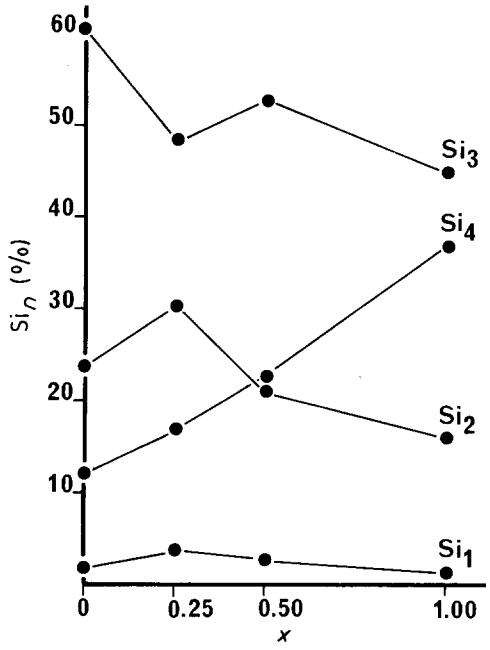

Figure 6 Evolution of the Si_n distribution on the T(2) site $\left(\sum_{n=1-4} Si_n = 100\right)$.

the number calculated for a random model, so indicating the existence of some short-range local order. This order, however, decreases with the increasing aluminium content because the $N_{Al-O-Al}$ observed/$N_{Al-O-Al}$ calculated ratio increases. This local order, which corresponds to a strong tendency for each silicon atom to be linked, through oxygen bridging, to a maximum number of aluminium atoms, is expressed in both tetrahedral sites by an important proportion of $Si_{3(Al)}$ or $Si_{4(Al)}$ atoms, clearly higher than the corresponding statistical values (Table VI and Fig. 6).

The evolution of the coordination of silicon atoms in the T(2)-site is particularly interesting to analyse. As shown in Table IV, each atom in the T(2)-site is linked to four atoms: two in the T(2)-site, two in the T(1)-site. The latter are essentially aluminium atoms because the T(1) sites are mainly occupied by aluminium atoms (Table V). Statistically the formers correspond either to one aluminium atom and one silicon atom (low potassium content: $Si_{3(Al)}$ dominant), forming within the 6-membered T(2) rings dissymmetric Al–O–Si–

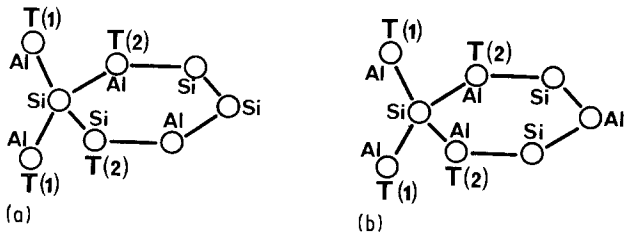

Figure 7 Schematic representation of the arrangement of Al/Si tetrahedra around silicon atom in T(2) site: (a) most probable distribution for low potassium (Si_3 dominant), (b) most probable distribution for high potassium content (Si_4 dominant).

O–Si–units in which the Si–O distance must be shorter than the Al–O distance, or to two aluminium atoms (high potassium content: $Si_{4(Al)}$ dominant) leading to symmetric –Al–O–Si–O–Al–units (see Fig. 7). This disparity in the T(2)–O(2) distances, which decreases with the increasing potassium content, is actually observed within each tetrahedron of the 6-membered rings.

In conclusion, MAS-NMR has shown to be of great value for elucidating the nature of local environment and the course of its change with increasing potassium content, in potassium substituted cordierite. Its application to the study of the evolution of this short-range order with the thermal treatment will be the subject of a forthcoming paper.

Appendix

Because each T(1)-site, occupied by α_1 Si and β_1 Al atoms ($\alpha_1 + \beta_1 = 3$), is surrounded by 4 T(2) sites, and each T(2)-site, occupied by α_2 Si and β_2 Al atoms ($\alpha_2 + \beta_2 = 6$), is surrounded by 2 T(2) and 2 T(1)-sites, the various probabilities Si_n^m ($m = 1, 2$; $n = 0, 1, 2, 3, 4$) for a given silicon atom, in T(m) site, to be linked to n aluminium atoms through oxygen bridging, are given as follows

$$Si_0^1 = \frac{\alpha_1}{3}\left(\frac{\alpha_2}{6}\right)^4$$

$$Si_0^2 = \frac{\alpha^2}{6}\left(\frac{\alpha_1\alpha_2}{18}\right)^2 \qquad \text{(A1)}$$

$$Si_1^1 = \frac{2\alpha_1\beta_2}{9}\left(\frac{\alpha_2}{6}\right)^3$$

$$Si_1^2 = 2\left[\left(\frac{\alpha_2}{6}\right)^2\frac{\alpha_1\beta_1}{9} + \left(\frac{\alpha_1\alpha_2}{18}\right)^2\frac{\beta_2}{6}\right] \quad \text{(A2)}$$

$$Si_2^1 = 2\alpha_1\left(\frac{\alpha_1\beta_2}{36}\right)^2$$

$$Si_2^2 = \frac{\alpha_2}{6}\left[\left(\frac{\alpha_1\beta_2 + \alpha_2\beta_1}{18}\right)^2 + \frac{2\alpha_1\alpha_2\beta_1\beta_2}{324}\right] \quad \text{(A3)}$$

$$Si_3^1 = \frac{2\alpha_1\alpha_2}{9}\left(\frac{\beta_2}{6}\right)^3$$

$$Si_3^2 = \frac{\alpha_1\alpha_2\beta_1}{27}\left(\frac{\beta_2}{6}\right)^2 + \frac{\beta_2}{3}\left(\frac{\alpha_2\beta_1}{18}\right)^2 \quad \text{(A4)}$$

$$Si_4^1 = \frac{\alpha_1}{3}\left(\frac{\beta_2}{6}\right)^4$$

$$Si_4^2 = \frac{\alpha_2}{6}\left(\frac{\beta_1\beta_2}{18}\right)^2 \quad \text{(A5)}$$

The intensities of the Si_n^m peaks are therefore given by

$$I_{Si_n^1} = \frac{3}{5 - x}Si_n^1 \quad \text{(A6a)}$$

and

$$I_{Si_n^2} = \frac{6}{5 - x}Si_n^2 \quad \text{(A6b)}$$

References

1. Y. H. KIM, J. P. MERCURIO and C. GAULT, *Ceram. Int.* **11** (1) (1985) 27.
2. P. THOMAS, J. P. MERCURIO and B. FRIT, *J. Mater. Sci. Lett.* **8** (1989) 52.
3. J. P. MERCURIO, D. MERCURIO, B. FRIT, Y. H. KIM and G. ROULT, *High Tech. Ceram. Mater. Sci. Monographs* **38** (1987) 361.
4. Y. H. KIM, D. MERCURIO, J. P. MERCURIO and B. FRIT, *Mater. Res. Bull.* **19** (1984) 209.
5. D. MERCURIO, P. THOMAS, J. P. MERCURIO, B. FRIT and G. ROULT, in "Proceedings of the 1st European Conference on Ceramics", Maastricht, 18–24 June (1989).
6. D. MERCURIO, P. THOMAS, J. P. MERCURIO, B. FRIT, Y. H. KIM, G. ROULT, *J. Mater. Sci.* **24** (1989) 76.
7. D. L. EVANS, G. R. FISCHER, J. E. GEIGER and F. W. MARTIN, *J. Amer. Ceram. Soc.* **63** (1980) 629.
8. M. F. HOCHELLA Jr. and G. E. BROWN Jr, *J. Amer. Ceram. Soc.* **69** (1) (1986) 13.
9. P. K. PREDECKI and J. HAAS, J. FABER Jr and R. L. HITTERMAN, *Adv. X-ray Anal.* **29** (1986) 173.
10. P. THOMAS, D. MERCURIO, J. P. MERCURIO and B. FRIT, *Europ. J. Solid State Inorg. Chem.* (to be published).
11. E. P. MEAGHER and G. V. GIBBS, *Can. Mineral.* **15** (1977) 43.
12. C. A. FYFE, J. M. THOMAS, J. KLINOWSKI and G. C. GOBI, *Angew. Chem. Int. Ed. Engl.* **22** (1983) 259.
13. C. A. FYFE, G. C. GOBI and A. PUTNIS, *J. Amer. Chem. Soc.* **108** (1986) 3218.
14. J. KLINOWSKI, S. W. CARR, S.E. TARLING and P. BARNES, *Nature* **330** (1987) 56.
15. A. PUTNIS, E. SALJE, S. A. T. REDFERN, C. A. FYFE and H. STROBL, *Phys. Chem. Minerals* **14** (1987) 446.
16. BRUKER, MSL Soft ware package.

Received 23 July 1990
and accepted 24 January 1991